Lasers in Manufacturing Conference 2023

Nano-steps to new functionalities: a laser-based process chain for oxide-dispersion strengthened steel

Mareen Goßling[a,*], Silja-Katharina Rittinghaus[a], Markus B. Wilms[a], Somnath Bharech[b], Yangyiwei Yang[b], Bai-Xiang Xu[b] and Bilal Gökce[a]

[a]*Chair of Materials Science and Additive Manufacturing, School of Mechanical Engineering and Safety Engineering, University of Wuppertal, Gaußstr. 20, 42119 Wuppertal, Germany*
[b]*Mechanics of Functional Materials Division, Institute of Materials Science, Technische Universität Darmstadt, Otto-Berndt-Strasse 3, 64287 Darmstadt, Germany*

Abstract

Oxide-dispersion strengthened (ODS) alloys are a prominent representative of metal matrix composites, highly demanded in high temperature and corrosive environments, e.g., efficient combustion engines. Conventional manufacturing of these materials is typically carried out by powder metallurgical processes, offering limited freedom in the fabrication of complex geometries. Additive manufacturing technologies allow the economical utilization of the cost-intensive powder material through direct near-net-shape manufacturing and thus significantly expand the range of applications.
In this study, the generation of spherical oxide nanoparticles (ZrO_2) by laser-based ablation in liquids (LAL) from bulk target material and subsequent deposition on gas-atomized steel powder (Fe-20Cr (wt.%)), a composite powder material suitable for the additive manufacturing process of laser powder bed fusion (PBF-LB/M) is produced. Thus, a complete laser-based additive manufacturing chain for metal-ceramic composites from powder particles to a final component is presented.

Keywords: Composite; ODS; Laser Ablation in Liquid; oxide; Laser Powder Bed Fusion; materials

1. Introduction

The expanding use of Additive Manufacturing (AM) in industry increases the demand for high-performance materials leading to intensified research activities in the field of materials tailored for AM. [1] However, the

* Corresponding author. Tel.: +0-000-000-0000 ; fax: +0-000-000-0000 .
E-mail address: author@institute.xxx .

laser powder bed fusion (PBF-LB) process, originally designed to process metals or polymers, is now also considered for the fabrication of metal-ceramic composite materials, uniting beneficial properties of both material types [2, 3]. High solidification rates [4] and highly dynamic melt pool flows [5] in AM processes hinder nanoparticles (NP) to agglomerate in the material's liquid state, thus the ceramic particles can be finely dispersed in the metallic matrix, which is a prerequisite for effective oxide dispersion-strengthening (ODS). [6]

ODS materials exhibit remarkable strength, especially under high-temperature conditions, particularly regarding creep [7, 8]. Therefore, they have attracted considerable attention in modern internal combustion engines [9] and are also candidates for use in novel nuclear power plants; due to their exceptional stability towards high-energy neutron radiation, they are also considered for future fusion power plants [10, 11].

ODS materials with AM have already been successfully manufactured[12], typically by utilizing powder composites produced by mechanical alloying (MA) [13–15]. However, the deformation-induced decrease in flowability [16, 17] results in smaller process windows [18], which created a demand for powder composites maintaining high sphericity. [19, 20] Electrostatic deposition (ED) in a liquid solvent enables pH-controlled NP deposition onto gas-atomized micrometre-sized metallic particles and has already been proven for yttrium oxide (Y_2O_3) to produce powder composites containing well suitable for different AM processes [21].

This work aims to improve ODS material functionalities by decreasing NP size and improving their distribution by a strongly laser-based process chain. Therefore, laser-generated ZrO_2 NPs, which promise to have a lower agglomeration behavior compared to Y_2O_3, are produced by LAL, supported onto binary Fe-20Cr (wt.%) alloy powder by ED and subsequently consolidated via PBF-LB/M.

2. Improving the strengthening effect of oxide particles in metals

Optimization of NP size and distance

The underlying strengthening mechanism in ODS is the Orowan mechanism. This mechanism occurs when dislocation movement is hindered by the presence of an incoherent second phase or precipitate particle in the material. In the investigated model material, Fe20Cr+0.8wt.%ZrO_2, ZrO_2 particles act as highly stable obstacles to the dislocation movement that has to be passed, which increases the material's strength and hardness. Equation (1) shows the parameters affecting the required shear stress for passing. The aim is to maximize this value, which can be achieved by reducing the particle size (radius r) and interparticle distance (l) in the ODS material.

$$\Delta\tau_{OR} = \frac{Gb}{l - 2r}$$

For reducing the particle size, LAL was used to produce very small and spherical NP (<10 nm). In addition, the size distribution of the NPs is very narrow, so inhomogeneity of mechanical properties due to different NP sizes can be avoided.

Improving powder processability

For a good flowability of the ODS powder, the ED method was used for additivation. In this process, the spherical base powder remains geometrically intact and the NPs are homogeneously applied to the powder particle surface by electrostatic attraction.

Considering melt pool dynamics

In the melt pool of AM processes, time-dependent forces such as gravity and buoyancy forces as well as recoil and Marangoni forces lead to turbulence [4, 22, 23], which is influenced by process parameters [24], among other things. In modelling approaches, buoyancy and gravitational forces of NPs in the melt pool are neglected, since due to NPs low mass a flow within the melt pool is assumed [25]. However, when NPs are

dispersed in the melt pool, they tend to agglomerate and aggregate strongly. This behavior is attributed to their large surface area, high interfacial energy with the surrounding molten metal, and van der Waals forces. The fast cooling rates in PBF-LB/M ensure quick solidification and little time in the liquid state for NP to agglomerate.

Identification of influencing variables by simulation

As NPs are particularly difficult to observe experimentally, simulation supports understanding NP movement and especially agglomeration behavior in the melt pool. Because of the material constant Hamaker, which influences the interparticle attraction, a lower agglomeration behavior can be expected for zirconia. This correlation is further elaborated for the thermophysical models described in [18, 26].

3. Results and discussion

3.1. NP agglomeration simulation during melt pool solidification in PBF-LB/M

A non-isothermal phase field model was used to simulate the Fe20Cr alloy microstructure evolution produced by the PBF-LB/M process. Based on this method an agglomeration statistics comparison between Y_2O_3 and ZrO_2 was done. The differences in agglomeration behavior can be attributed to the material-dependent Hamaker constant, which results in different van der Waals forces between two NPs in the melt pool during solidification. Results show that especially within the grains Y_2O_3 NPs have an increased tendency to agglomerate compared to ZrO_2 NPs. In total, 32.7 % of Y_2O_3 particles are involved in agglomeration, compared to 25.8 % of ZrO_2 particles. A lower NP proportion in agglomeration after solidification of the melt leads to a better NP distribution in the component, which increases the material strength according to equation (1). The applied models thus imply, that ZrO_2 promises to result in decreased agglomeration compared to Y_2O_3.

3.2. NPs generated via LAL

In LAL, a laser beam is focused on a target which is surrounded by liquid. The ablated material is converted into a plasma phase during irradiation with a laser pulse. [27] By reaching the ablation threshold, NPs are removed from the target surface and carried away by the flowing liquid. In addition to the surrounding liquid (deionized water, DI) and the laser parameters, it is primarily the target material that influences the chemical NP composition. To generate the ZrO_2 NPs, a Zr700 (VDM Metals, Altona, Germany) target material was ablated in DI-water with a 1060 nm ytterbium pulsed fibre laser(YLPN-0.5-1×5-80, IPG Laser GmbH) with 61 W, a 1 ns pulse duration and 3 MHz repetition rate. To circulate the liquid, a peristaltic pump LabV3 (Baoding Shenchen Precision Pump Co. Ltd, Baoding, China) with a constant 150 ml/min flow rate was used.

The LAL-generated NPs feret diameter size distribution is shown in Figure 1a). The particle size distribution is relatively narrow and monodisperse with an average diameter of 3.6 nm. Smaller NPs lead to a higher number of oxide particles for identical introduced amounts (wt.-%) in the final ODS part and are highly beneficial for the Orowan strengthening effect, also due to lower interparticle distances.

The EDS line scan of an individual oxide particle is shown in Figure 1b). The Zr and oxygen signal increases proportionally with the particle diameter, indicating an even distribution. In addition, hafnium is detected, which is already present as an impurity in the base target material. The low chromium and iron signals can be interpreted as background noise. The EDS mapping showed a percentage of 22.1 at.-% Zr, 72.7 at.-% O and 4.2 at.-% Hf with a 1 at.-% residual. This is an indication of the zirconium oxide formation.

For further characterization of the NPs X-ray diffraction was used. The reflections of ZrO_2, those of pure Zr as well as orthorhombic and monoclinic HfO_2 are detected. Monoclinic HfO_2 reflections are partially present without interference with ZrO_2 reflections or the other phases. It can be concluded that monoclinic HfO_2 is

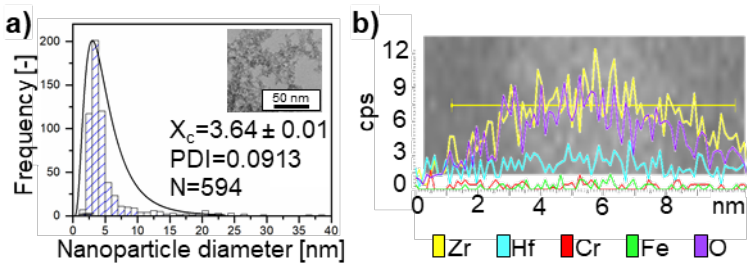

Fig. 1. (a) NP Feret diameter size distribution derivded by TEM image processing; (b) EDS line scan of LAL generaded NP

present in addition to tetragonal ZrO_2. This is also true for reflections of orthorhombic HfO_2, but these show a much lower intensity compared to monoclinic HfO_2.

3.3. Oxide additivated metal powder

The ZrO_2-NP were supported on gas atomized Fe20Cr (wt.%) metal powder (Rosswag GmbH, Pfinztal, Germany) with a size 15 µm to 45 µm distribution (d_{10} = 19 µm, d_{50} = 29 µm, d_{90} = 43 µm) by ED in a solution. The metal base material moisture content was 0.08 wt.-% H_2O, remaining moisture in the oxide additivated metal powder after deposition is 0.12 wt.-% H_2O.

The NP supporting leads to a homogenous NP distribution on the metal powder, which is exemplarily shown in Figure 2. Figure 2a) shows a complete oxide-supported metal powder particle. In the close-up in Figure 2b), bright areas on the powder particle surface can be seen, indicating the ZrO_2 NPs presence, which is also confirmed by the SEM-EDS spectra of Zr in c) and O in d). A uniform Zr distribution is detected, while in certain areas a stronger Zr signal is measured, suggesting a ZrO_2 accumulation. Overall, a homogeneous NP distribution on the entire powder surface with some large (<1µm) and a high number of small (<100 nm) agglomerates or individual particles can be deduced.

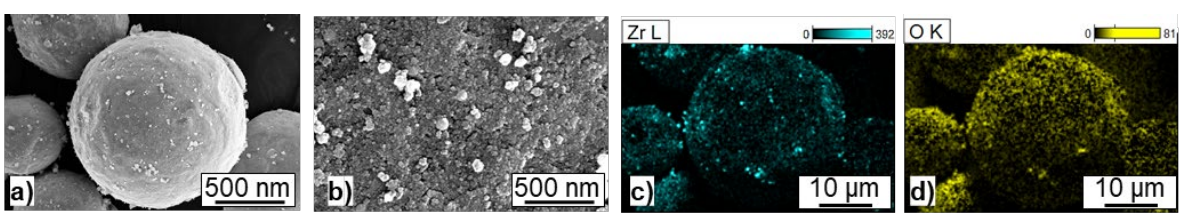

Fig. 2. SEM images of oxide supported metal powder; (a),(b) SEM image of particle in different magnification; (c) EDS Zr signal; (d) EDS O signal

3.4. Consolidated Fe20Cr and Fe20Cr+0.8 wt.-% ZrO_2

Both the Fe20Cr (wt.-%) base powder and the oxide additivated metal powder were consolidated on a 316L substrate plate via PBF-LB/M (Aconity3D GmbH, Herzogenrath, Germany) in an argon atmosphere. The laser (λ=1064 nm) focal spot is 48 µm in diameter. The applied volume energy density (VED) of 78 J/mm³ was calculated from 150 W laser power (P_L), 800 mm/s scan velocity (v_s) and 80 µm hatch distance (D_s) with a

30 µm layer height (Δz_s). The relative density of the Fe20Cr sample of 99.7 % is slightly higher compared to the one of the ODS sample with a measured value of 98.3 %. One suspected cause is the remaining moisture content in the ODS sample due to the supporting route, which might form pores during its evaporation.

Detecting the NP distribution in the printed component is challenging due to the small NP size. In Figure 3, cross-sections of etched samples are shown. It is assumed that the NPs protrude in the etched state of the ODS sample and thus appear as bright spots in the SEM image. To investigate this hypothesis, SEM-EDS measurements were performed. The results for the Zr content are listed in Table 1. Bright spots are also visible on the surface of the unmodified Fe20Cr sample, but taking into account the statistical error no Zr was detected in these (Table 1, area 1-4), while clearly increased contents are detected for similar spots in the ODS samples (Table 1, area 5 and 7), indicating NP agglomerates. In comparison, the bright spots in the SEM image of the ODS sample are visibly smaller and more homogeneously distributed. However, it has to be mentioned that an increased Zr content on the whole sample is detected by EDS, also in the darker areas (Figure 3h) and Table 1, areas 6 and 8) owing to smaller, visually unresolved NPs.

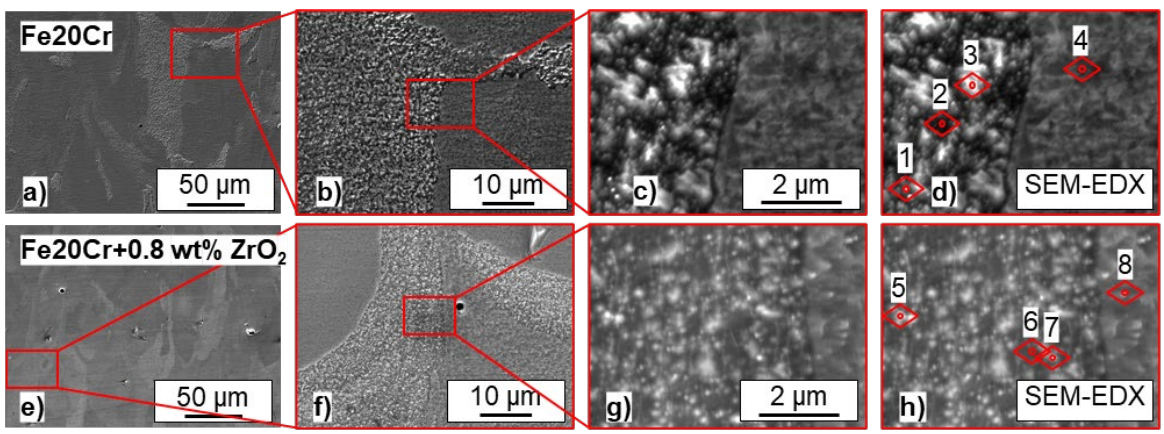

Fig. 3. SEM images of cross sections of PBF-LB/M-built parts of Fe20Cr (a)-d) and Fe20Cr-0.8 ZrO2 (e)-h), in etched state; SEM-EDS mapping d),h).

Table 1. SEM- EDS spectra of Fe20Cr and ODS-sample

	Fe20Cr				Fe20Cr+0.8wt.-%ZrO2			
Area	1	2	3	4	5	6	7	8
Zr [wt.%]	0.05	0.04	0.07	0.06	0.8	0.18	0.88	0.15

4. Conclusion

This study presents the viability of a fully laser-based process approach for ODS steels. Through the utilization of Laser Ablation in Liquid, ZrO_2 NPs with an average particle diameter of 3.6 nm were successfully produced. Additionally, ED was employed to effectively introduce ZrO_2 into a homogeneous Fe20Cr-base powder, while preserving the powder's flowability. Consequently, samples with a density exceeding 98% could be fabricated.

Simulations have revealed that the composition of the NPs themselves plays a crucial role in the agglomeration behavior and subsequent distribution of the NPs within the solidified component. By achieving a homogeneous dispersion of small, predominantly individual NPs, or agglomerates below 10 nm, it is anticipated that the strength of the ODS composite material will surpass the current state-of-the-art.

Future investigations will primarily focus on determining the functional mechanical properties of the ODS material and gaining a comprehensive understanding of the interdependencies between processing parameters and NP behavior.

Acknowledgements

This study is part of a research project funded by the German Research Foundation (DFG) under Priority Program 2122 "Materials for Additive Manufacturing" (SPP 2122, project number 493889809, GO 2566/13-1). B. Gökce additionally acknowledges funding from the DFG within the Heisenberg Program, project GO 2566/10-1 (445127149). The authors would like to express their sincere gratitude to several individuals who contributed to the successful completion of this study. We thank Prof. Matthias Epple for the use of their SEM, Louis Becker for the SEM and EDS measurements of the consolidated samples as well as XRD of the NPs and Daniel Behrens for his assistance with experimental tasks. Finally, S. Bharech, Y. Yang and B.-X. Xu greatly appreciates the access to the Lichtenberg II High-Performance Computer (HPC) and the technique supports from the HHLR, Technical University of Darmstadt. The computation time on the HPC is granted by the NHR4CES Resource Allocation Board under the project "special00007''.

References

1 Pollock, T.M., Clarke, A.J., Babu, S.S. (2020) Design and Tailoring of Alloys for Additive Manufacturing. *Metall Mater Trans A*, **51** (12), 6000–6019.

2 AlMangour, B., Baek, M.-S., Grzesiak, D., Lee, K.-A. (2018) Strengthening of stainless steel by titanium carbide addition and grain refinement during selective laser melting. *Materials Science and Engineering: A*, **712**, 812–818.

3 Gu, D., Wang, H., Zhang, G. (2014) Selective Laser Melting Additive Manufacturing of Ti-Based Nanocomposites: The Role of Nanopowder. *Metall and Mat Trans A*, **45** (1), 464–476.

4 Hooper, P.A. (2018) Melt pool temperature and cooling rates in laser powder bed fusion. *Additive Manufacturing*, **22**, 548–559.

5 Guo, Q., Zhao, C., Qu, M., Xiong, L., Hojjatzadeh, S.M.H., Escano, L.I., Parab, N.D., Fezzaa, K., Sun, T., Chen, L. (2020) In-situ full-field mapping of melt flow dynamics in laser metal additive manufacturing. *Additive Manufacturing*, **31**, 100939.

6 Yu, W.H., Sing, S.L., Chua, C.K., Kuo, C.N., Tian, X.L. (2019) Particle-reinforced metal matrix nanocomposites fabricated by selective laser melting: A state of the art review. *Progress in Materials Science*, **104**, 330–379.

7 Bartsch, M., Wasilkowska, A., Czyrska-Filemonowicz, A., Messerschmidt, U. (1999) Dislocation dynamics in the oxide dispersion strengthened alloy INCOLOY MA956. *Materials Science and Engineering: A*, **272** (1), 152–162.

8 Brandes, M.C., Kovarik, L., Miller, M.K., Daehn, G.S., Mills, M.J. (2012) Creep behavior and deformation mechanisms in a nanocluster strengthened ferritic steel. *Acta Materialia*, **60** (4), 1827–1839.

9 Min, Z., Parbat, S.N., Yang, L., Kang, B., Chyu, M.K. (2018) Fabrication and Characterization of Additive Manufactured Nickel-Based Oxide Dispersion Strengthened Coating Layer for High-Temperature Application. *Journal of Engineering for Gas Turbines and Power*, **140** (6).

10 Gao, J., Song, P., Huang, Y.-J., Yabuuchi, K., Kimura, A., Sakamoto, K., Yamashita, S. (2019) Effects of neutron irradiation on 12Cr–6Al-ODS steel with electron-beam weld line. *Journal of Nuclear Materials*, **524**, 1–8.

11 Lu, C., Lu, Z., Wang, X., Xie, R., Li, Z., Higgins, M., Liu, C., Gao, F., Wang, L. (2017) Enhanced Radiation-tolerant Oxide Dispersion Strengthened Steel and its Microstructure Evolution under Helium-implantation and Heavy-ion Irradiation. *Sci Rep*, **7** (1).

12 Wilms, M.B., Rittinghaus, S.-K., Goßling, M., Gökce, B. (2023) Additive manufacturing of oxide-dispersion strengthened alloys: Materials, synthesis and manufacturing. *Progress in Materials Science*, **133**, 101049.

13 Walker, J.C., Berggreen, K.M., Jones, A.R., Sutcliffe, C.J. (2009) Fabrication of Fe-Cr-Al Oxide Dispersion Strengthened PM2000 Alloy Using Selective Laser Melting. *Adv. Eng. Mater.*, **11** (7), 541–546.

14 Boegelein, T., Louvis, E., Dawson, K., Tatlock, G.J., Jones, A.R. (2016) Characterisation of a complex thin walled structure fabricated by selective laser melting using a ferritic oxide dispersion strengthened steel. *Materials Characterization*, **112**, 30–40.

15 Wilms, M.B., Streubel, R., Frömel, F., Weisheit, A., Tenkamp, J., Walther, F., Barcikowski, S., Schleifenbaum, J.H., Gökce, B. (2018) Laser additive manufacturing of oxide dispersion strengthened steels using laser-generated nanoparticle-metal composite powders. *Procedia CIRP*, **74**, 196–200.

16 Suryanarayana, C., Klassen, T., Ivanov, E. (2011) Synthesis of nanocomposites and amorphous alloys by mechanical alloying. *J Mater Sci*, **46** (19), 6301–6315.

17 Park, J.J., Hong, S.M., Park, E.K., Lee, M.K., Rhee, C.K. (2012) Synthesis of Fe based ODS alloys by a very high speed planetary milling process. *Journal of Nuclear Materials*, **428** (1-3), 35–39.

18 Vasquez, E., Giroux, P.-F., Lomello, F., Nussbaum, M., Maskrot, H., Schuster, F., Castany, P. (2020) Effect of powder characteristics on production of oxide dispersion strengthened Fe 14Cr steel by laser powder bed fusion. *Powder Technology*, **360**, 998–1005.

19 Spurek, M.A., Haferkamp, L., Weiss, C., Spierings, A.B., Schleifenbaum, J.H., Wegener, K. (2021) Influence of the particle size distribution of monomodal 316L powder on its flowability and processability in powder bed fusion. *Prog Addit Manuf*.

20 Doñate-Buendía, C., Gu, D., Schmidt, M., Barcikowski, S., Korsunsky, A.M., Gökce, B. (2021) On the selection and design of powder materials for laser additive manufacturing. *Materials & Design*, **204**, 109653.

21 Gökce, B., Streubel, R., Wilms, M., Schleifenbaum, J.H., Barcikowski, S. (2019) Laser additive manufacturing of oxide dispersion strengthened steels (Conference Presentation), **10909**, SPIE.

22 Singh, A.K., Mundada, Y., Bajaj, P., Wilms, M.B., Patil, J.P., Mishra, S.K., Jägle, E.A., Arora, A. (2022) Investigation of temperature distribution and solidification morphology in multilayered directed energy deposition of Al-0.5Sc-0.5Si alloy. *International Journal of Heat and Mass Transfer*, **186**, 122492.

23 Bidare, P., Bitharas, I., Ward, R.M., Attallah, M.M., Moore, A.J. (2018) Fluid and particle dynamics in laser powder bed fusion. *Acta Materialia*, **142**, 107–120.

24 Gu, D., Ma, C., Xia, M., Dai, D., Shi, Q. (2017) A Multiscale Understanding of the Thermodynamic and Kinetic Mechanisms of Laser Additive Manufacturing. *Engineering*, **3** (5), 675–684.

25 Ozsoy, I.B., Li, G., Choi, H., Zhao, H. (2015) Shape effects on nanoparticle engulfment for metal matrix nanocomposites. *Journal of Crystal Growth*, **422**, 62–68.

26 Yang, Y., Kühn, P., Yi, M., Egger, H., Xu, B.-X. (2020) Non-isothermal Phase-Field Modeling of Heat–Melt–Microstructure-Coupled Processes During Powder Bed Fusion. *JOM*, **72** (4), 1719–1733.

27 Fazio, E., Gökce, B., Giacomo, A. de, Meneghetti, M., Compagnini, G., Tommasini, M., Waag, F., Lucotti, A., Zanchi, C.G., Ossi, P.M., Dell'Aglio, M., D'Urso, L., Condorelli, M., Scardaci, V., Biscaglia, F., Litti, L., Gobbo, M., Gallo, G., Santoro, M., Trusso, S., Neri, F. (2020) Nanoparticles Engineering by Pulsed Laser Ablation in Liquids: Concepts and Applications. *Nanomaterials*, **10** (11).